Uptake mechanisms of selenium oxyanions during the ferrihydrite-hematite recrystallization

Börsig, N.; Scheinost, A. C.; Shaw, S.; Schild, D.; Neumann, T.;

Uptake mechanisms of selenium oxyanions during the ferrihydrite-hematite recrystallization

Nicolas Börsig [a,*], Andreas C. Scheinost [b,c], Samuel Shaw [d], Dieter Schild [e], Thomas Neumann [a]

[a] Karlsruhe Institute of Technology (KIT), Institute of Applied Geosciences, Adenauerring 20b, 76131 Karlsruhe, Germany

[b] Helmholtz-Zentrum Dresden - Rossendorf (HZDR), Institute of Resource Ecology, Bautzner Landstraße 400, 01328 Dresden, Germany

[c] The Rossendorf Beamline (ROBL) at ESRF, 38043 Grenoble, France

[d] The University of Manchester, School of Earth, Atmospheric and Environmental Sciences, Manchester, M13 9PL, United Kingdom

[e] Karlsruhe Institute of Technology (KIT), Institute for Nuclear Waste Disposal, Hermann-von-Helmholtz-Platz 1, 76344 Eggenstein-Leopoldshafen, Germany

* Corresponding author: Tel.: +49 721 608-44878; nicolas.boersig@kit.edu (N. Börsig)

Abstract

Se is an essential nutrient at trace levels, but also a toxic environmental contaminant at higher concentrations. The mobility of the trace element Se in natural environments is mainly controlled by the occurrence of the highly soluble Se oxyanions – selenite [Se(IV)] and selenate [Se(VI)] - and their interaction with geological materials. Since iron oxides are ubiquitous in nature, many previous studies investigated Se retention by adsorption onto iron oxides. However, little is known about the retention of Se oxyanions during the formation process of iron oxides. In this paper, we therefore studied the immobilization of Se oxyanions during the crystallization of hematite from ferrihydrite. In coprecipitation studies, hematite was synthesized by the precipitation and aging of ferrihydrite in an oxidized Se(IV)- or Se(VI)-containing system (pH 7.5). Hydrochemical data revealed the complete uptake of all available Se(IV) up to initial concentrations of 10^{-3} mol/L (m/V ratio = 9.0 g/L), while the retention of Se(VI) was extremely low (max. 15 %). In case of high initial Se(IV) concentrations, the results also demonstrated that the interaction of Se with ferrihydrite can affect the type of the final transformation product. Comparative adsorption studies, performed at identical conditions, allowed a distinction between pure adsorption and coprecipitation and

showed a significantly higher Se retention by coprecipitation than by adsorption. Desorption studies indicated that Se coprecipitation leads to the occurrence of a resistant, non-desorbable Se fraction. According to time-resolved studies of Se(IV) or Se(VI) retention during the hematite formation and detailed spectroscopic analyses (XPS, XAS), this fraction is the result of an incorporation process, which is not attributable to Fe-for-Se substitution or the Se occupation of vacancies. Se initially adsorbs to the ferrihydrite surface, but after the transformation of ferrihydrite into hematite, it is mostly incorporated by hematite. In systems without mineral transformation, however, Se remains as a sorption complex. In case of Se(VI), an outersphere complex forms, while Se(IV) forms a mixture of bidentate mononuclear edge-sharing and bidentate binuclear corner-sharing inner-sphere complexes. The results of this study demonstrate that occlusion of Se oxyanions by hematite is an important retention mechanism, in addition to pure adsorption, for immobilizing Se in natural systems, which may control Se migration processes in polluted environments.

1   Introduction

Selenium (Se) is a trace element of special concern, since it is an essential nutrient for organisms at low concentrations, but a toxic contaminant at slightly higher concentrations (Lenz and Lens, 2009). Of concern are therefore not only Se-deficient agricultural soils in certain regions of the World, but also Se contaminations of soils or wastewaters (Dhillon and Dhillon, 2003; Lenz and Lens, 2009; Christophersen et al., 2012). In addition, Se occurs in vitrified high-level nuclear waste (HLW) in the form of the long-lived, harmful radionuclide [79]Se (Cannière et al., 2010). In soils in contact with the atmosphere, the dominant Se species are the oxyanions selenate [Se(VI)] and selenite [Se(IV)]; Se(IV) is also the expected predominant Se species in vitrified HLW (Bingham et al., 2011). These higher Se oxidation states are of particular concern for the biogeochemical behavior of Se in soils and waters, since they form species with high solubility (Séby et al., 2001) which, in turn, is responsible for a high environmental mobility, bioavailability and toxicity (Dhillon and Dhillon, 2003; Lenz and Lens, 2009). For the same reason, Se oxyanions play a major role in the long-term safety assessment of HLW repositories. In this case, migration into the geo/biosphere cannot be fully excluded for Se oxyanions, due to their restricted retention by the engineered and natural barriers (Séby et al., 1998; Mallants et al., 2001; Bingham et al., 2011), although recent research has demonstrated that Se occurs as Se(-II) in burnt nuclear fuel (Curti et al., 2014; Curti et al., 2015) and is furthermore easily reduced to Se(-II) or Se(0) by Fe(II)-

bearing minerals on steel container surfaces (Scheinost and Charlet, 2008; Scheinost et al., 2008). The fate of dissolved Se(IV) and Se(VI) species in subsurface systems is often determined by interaction with mineral phases, including processes such as adsorption, incorporation and reductive precipitation, which are key immobilization mechanisms (Chen et al., 1999; Grambow, 2008). In this context, crystalline iron (oxyhydr)oxides minerals (e.g. hematite and goethite) and their precursors (e.g. ferrihydrite) are of great importance as they are widespread in nature and capable of anion sorption (Roh et al., 2000; Sparks, 2003; Adegoke et al., 2013).

The mechanism of Se adsorption to iron oxide surfaces has been investigated in detail by a number of previous studies. They show that adsorption of Se(IV) and Se(VI) onto iron oxides can be very efficient at lower pH, but is limited under near-neutral and alkaline pH conditions (e.g. Balistrieri and Chao, 1990; Zhang and Sparks, 1990; Parida et al., 1997; Duc et al., 2003; Martínez et al., 2006; Rovira et al., 2008). This tendency is independent of the type of iron oxide, since alkaline conditions generally lead to the formation of a negative charge at the iron oxide surface and therefore to a poor adsorption of anionic species (Fernández-Martínez and Charlet, 2009). Moreover, the adsorption of Se(IV) to all iron oxides is generally higher and there is little release with increasing ionic strength, whereas the adsorption of Se(VI) is much lower and strongly influenced by the presence of competing anions (Hayes et al., 1987; Su and Suarez, 2000; Rietra et al., 2001; Jordan et al., 2013; Jordan et al., 2014). Most authors suggest the difference between Se(IV) and Se(VI) adsorption is due to the nature of the chemical attachment and the formation of different types of adsorption complexes. Spectroscopic investigations as well as surface complexation modeling reveal that the adsorption of Se(IV) onto iron oxides is usually the result of inner-sphere complexation (Fernández-Martínez and Charlet, 2009) with a mostly bidentate character, e.g. for hematite (Catalano et al., 2006; Duc et al., 2006). By contrast, the poor adsorption of Se(VI) and the strong impact of competing anions has been attributed to the formation of outer-sphere complexes (Hayes et al. 1987). However, more recent studies suggest that adsorption Se(VI) can occur via both inner-sphere and outer-sphere complexation (Peak and Sparks, 2002; Wijnja and Schulthess, 2002; Jordan et al., 2013). The type of surface complexation depends on pH, ionic strength, the nature of the iron oxide mineral and its surface loading (Peak and Sparks, 2002; Fukushi and Sverjensky, 2007; Fernández-Martínez and Charlet, 2009). A the results of a range of studies of the Se(VI) adsorption mechanisms onto goethite, ferrihydrite or hematite (Manceau and Charlet, 1994; Rietra et al., 2001; Peak and Sparks, 2002; Wijnja and

Schulthess, 2002; Fukushi and Sverjensky, 2007; Das et al., 2013) remain to some extent contradictory.

In addition, there is to the best of our knowledge no research available investigating the possible role of the incorporation of Se oxyanions into iron oxide minerals. The incorporation of anionic trace elements by iron oxides was demonstrated in several publications. These studies revealed oxyanion incorporation or occlusion by hematite for Si(IV) by hematite (Liu et al., 2012), P(V) (Gálvez et al., 1999a; Gálvez et al., 1999b), As(V) (Bolanz et al., 2013), V(V) (Sracek, 2015) and Tc(VII) (Skomurski et al., 2010). For this reason, it is conceivable that a retention mechanism on the basis of incorporation also exists for the both Se oxyanions, Se(IV) and Se(VI). However, incorporation can only be relevant in cases where iron oxide phases interact with Se oxyanions during their formation or transformation, including recrystallization or sorption induced crystal growth. Since the formation pathway of crystalline iron oxides commonly includes amorphous metastable intermediates (e.g. ferrihydrite, Cornell and Schwertmann, 2003), such processes are very common in natural systems and can be crucial for the mobility and transport behavior of dissolved Se species within contaminated sites as well as the critical zone (e.g. Bajaj et al., 2011). Hematite [α-Fe_2O_3], as one of the most stable and widespread iron oxides in nature (Cornell and Schwertmann, 2003), usually results from amorphous ferrihydrite that recrystallizes into hematite after a certain period of time by phase transformation and particle growth (Cornell and Schwertmann, 2003; Adegoke et al., 2013; Soltis et al., 2016). In the environment of HLW disposal sites, hematite can occur as a primary mineral phase in the host rock formation or the barrier materials (Duc et al., 2006). Since the hydrochemical conditions of an HLW repository are predicted to be reducing a few years after closure (Grambow, 2008; Iida et al., 2009), the interaction of Se oxyanions with freshly formed ferrihydrite and its alteration product hematite under oxidizing conditions would correspond to a worst-case scenario where Se is rapidly released from the waste forms.

The aim of our work was, therefore, to determine whether the incorporation of Se oxyanions into hematite can occur under a range of geochemical conditions. For this, we characterized the interaction of Se oxyanions with hematite during its crystallization from ferrihydrite via coprecipitation experiments, and compared these results with those from Se adsorption to ferrihydrite and hematite. In contrast to many previous Se adsorption studies, all experiments were conducted at a near-neutral pH and thus under conditions that are more comparable to natural systems. Through the combination of hydrochemical data and a detailed analysis of

the solid phases via X-Ray Diffraction (XRD), Scanning Electron Microscopy (SEM), X-ray Photoelectron Spectroscopy (XPS) and X-ray Absorption Spectroscopy (XAS), it was possible for the first time to prove the presence of an incorporated Se fraction within hematite, to identify the nature of the Se retention mechanism and to differentiate between Se coprecipitation and adsorption in terms of retention capacity and stability. These results provide useful information about long-term Se immobilization mechanisms in addition to pure adsorption, providing contributions to the safety assessments of HLW repositories as well as to a better global understanding of the Se retention processes in contaminated areas or in the critical zone.

2   Materials and Methods

2.1   Materials

All solutions were made of analytically pure grade chemicals and de-ionized Milli-Q water (18.2 $M\Omega cm^{-1}$). The Se stock solutions used in the coprecipitation and adsorption experiments were prepared by dissolving defined quantities of Na_2SeO_3 or $Na_2SeO_4 \cdot 10\,H_2O$ in Milli-Q water to receive total Se(IV) or Se(VI) concentrations of 0.1 mol/L and 1.0 mol/L.

2.2   Preparation of synthetic hematite and ferrihydrite

Hematite (Hm) was synthesized in the laboratory by using a slightly modified method of Schwertmann and Cornell (2000) in order to reflect formation of hematite from ferrihydrite (Fh) under conditions that are more comparable to natural than to laboratory conditions in terms of the main hydrochemical parameters. This implies the prerequisite that the mineral formation took place in an aquatic aerobic system under neutral to slightly alkaline pH conditions and at moderate temperatures. Hematite was synthesized by dissolving 40 g $Fe(NO_3)_3 \cdot 9\,H_2O$ in 500 ml Milli-Q water. After the addition of 300 ml 1 M KOH and the immediate precipitation of ferrihydrite (red-brownish compound), the suspension was titrated and buffered with 50 ml of 1 M $NaHCO_3$ solution before the final pH of 7.5 was adjusted with additional 25 ml of 1 M KOH. All solutions were preheated to temperatures of 50°C and stirred continuously during the mixing. Afterwards, the flask was sealed and the prepared suspension stored in an oven at 50°C for 10 days. Slightly increased temperatures of 50°C were chosen to favor transformation of ferrihydrite into hematite rather than goethite, and to speed up the mineral transformation processes (Schwertmann et al. 2004, Clay Miner. 39, 433-438). The procedure for the synthesis of ferrihydrite was identical, except that the

5

reaction was terminated after 1 hour. With approx. 8 g precipitated iron oxide froming, the mass to volume ratio (m/V) between hematite/ferrihydrite and the aqueous solution was approx. 9.0 g/L during these batch experiments. At the end of the respective reaction time, the precipitates were decanted and centrifuged. While a sample of the solutions was taken for the analysis of the Fe concentration and pH, the solids were washed 3 times with Milli-Q water to remove NO_3^- and HCO_3^- impurities. Synthesized hematite samples were then dried at moderate temperatures of 40°C, while ferrihydrite samples were freeze-dried to avoid re-crystallization processes. After that, the aggregated particles were ground with an agate mortar and stored until the analysis or the use in subsequent experiments.

2.3   Selenium coprecipitation studies

Since Se(IV) or Se(VI) speciation during the coprecipitation experiment is controlled by the hydrochemical conditions during the hematite synthesis, the procedure of sample preparation was almost identical to the synthesis of pure hematite. To investigate the Se(VI) and Se(VI) uptake by coprecipitation, different volumes of Se stock solutions were added to the dissolved Fe^{3+} prior to the beginning of the first mineral precipitation. Furthermore, the residual Se concentrations after the experiments were analyzed and a part of the solid sample was dried without prior washing with Milli-Q water in order to preserve the surface characteristics of the sample. Added Se stock solution volumes were calculated to obtain initial Se concentrations of 10^{-4} - 10^{-2} mol/L after the mixing of all solutions (m/V ratio = 9.0 g/L). These relatively high Se concentrations reflect extreme natural amounts but were necessary to increase the Se percentage within the solid iron oxide samples in order to improve the Se detection for the subsequent analyses. Different initial Se concentrations were used to vary the Fe/Se ratios in the solid samples.

Time-resolved investigations of the re-crystallization of hematite were carried out to examine the role of the precursor phase ferrihydrite onto Se retention. For this, samples of both the solid precipitate and the solution were collected and analyzed after several time intervals (10 min, 1 h, 6 h, 1 d, 2 d, 4 d, 6 d, 8 d, 10 d) during the hematite formation process.

2.4   Selenium adsorption studies

For comparison with the coprecipitation experiments, we studied also Se adsorption on pure hematite in batch experiments. The experimental settings were kept similar to the conditions at the end of the coprecipitation experiments. This mainly includes the parameters pH, ionic strength and the m/V ratio. The ionic strength was calculated under the assumption that the

extremely low solubility of hematite at pH 7.5 leads to the precipitation of the entire initial Fe(III) quantity, resulting in a residual ionic strength of 0.43 mol/L. Since the synthesis is mainly based on the use of $Fe(NO_3)_3$ and KOH solutions, the ionic strength is determined primarily by KNO_3.

For the investigation of the Se(IV) and Se(VI) uptake by adsorption as a function of the initial Se concentrations in the range 10^{-4} - 10^{-2} mol/L, 40 ml of 0.43 M KNO_3, which contained a defined volume of a Se stock solution, was added to 361.8 mg of pure hematite powder in sealable flasks followed by an adjustment of the pH to 7.5 by dropwise addition of either 0.1 M HNO_3 or KOH solutions. Afterwards, the flasks were sealed and shaken for 48 hours to ensure that an adsorption equilibrium was achieved. Due to the strong buffer ability of the hematite, the pH was checked after 24 and 45 hours and if necessary adjusted again to pH 7.5. The subsequent treatment of the samples was identical to the procedure after the coprecipitation studies. This approach allowed the preparation of hematite samples with varying content of adsorbed Se.

In addition to the adsorption studies with varying initial Se concentrations, some further similar experiments were carried out to study the Se(IV) and Se(IV) adsorption onto hematite depending on pH and the ionic strength. This provides information on the specific effect of the pH value and the background electrolyte concentration for the interaction processes during the mineral formation.

2.5 Desorption studies

Se(IV) and Se(VI) desorption was investigated by two procedures to characterize and compare the stability of the retention mechanisms. In the first procedure, batch experiments were carried by mixing a specific amount of dried hematite powder from previous Se adsorption or coprecipitation studies with the desorption solution in the ratio m/V = 9.0 g/L. The desorption solution was made of 0.01 M KNO_3 with a pH of 12 (adjusted with KOH) to exploit the limited adsorption capacity of hematite under alkaline conditions and to achieve a maximum removal of adsorbed Se from the hematite surface. The pH was still low enough to avoid the dissolution of the hematite phase. After mixing, the suspensions were shaken for 24 hours, then centrifuged and decanted. The residual supernatants were filtered, before pH was measured and the Se and Fe concentration in the aqueous phase was analyzed. This procedure was repeated three times and the total amount of removed Se was calculated as the sum of

each desorption step. This desorption studies enabled also the preparation of hematite samples with a low fraction of adsorbed Se(IV) or Se(VI).

In the second procedure, desorption of Se(IV) from selected iron oxides samples was studied as a function of OH^- concentration. The used technique is based on a method of Doornbusch et al. (2015) for iron oxide dissolution, but was adjusted for use under alkaline conditions. For this purpose, a specific amount of Se-bearing iron oxide powder was treated several times with NaOH of various concentrations (m/V = 3.4 g/L). NaOH was used to obtain lower total ionic strengths compared to KOH, in order to reduce analytical difficulties and to enable the use of higher OH^- concentration. In each step the mixture was allowed to react for 30 min, before the suspension was centrifuged and a sample of the supernatant was collected for Fe and Se analysis. The remaining supernatant was then discarded and replaced by the next higher OH^- solution. Overall, 8 desorption steps with increasing OH^- concentrations of 10^{-5}, 10^{-4}, 0.001, 0.005, 0.01, 0.05, 0.1 and 0.5 mol/L were used to study the effect of $[OH^-]$ on the desorption behavior. After the last NaOH solution, the remaining solid was reacted with 6 M HCl for 48 h to completely dissolve the iron oxide. This allowed the determination of the total Se and Fe contents of the solid phase.

2.6   Analytical techniques

2.6.1   Dissolved selenium and iron concentrations

After centrifugation and filtration (0.2-µm filter), all supernatants were acidified with concentrated high-purity HNO_3 (50 µL). The Se and Fe concentrations in the aqueous phase were determined by ICP-OES (Inductively Coupled Plasma Optical Emission Spectrometry) or ICP-MS (Inductively Coupled Plasma Mass Spectrometry) depending on the concentrations: For amounts higher than 1 mg/L, measurements were performed on ICP-OES using a Varian 715ES. Analysis of samples with lower Fe and Se concentrations were carried out on an X-Series 2 ICP-MS (Thermo Fisher Scientific Inc.). Collision cell mode was used to eliminate polyatomic clusters, and Se and Fe isotopes (m/z: 76, 77, 78 for Se; 56 for Fe) without spectroscopic interferences were selected for detection. ^{45}Sc, ^{103}Rh and ^{115}In were used as internal standards to minimize non-spectroscopic interferences. This includes the correction of signal changes caused by high ionic strength in some of the sample matrices. The lower detection limits were approx. 1 µg/L for both Se and Fe. Throughout the analysis of both ICP methods, a certified reference solution was used as standard.

2.6.2 Characterization of the solid phases

At the end of each batch experiment, the dried solid samples were characterized by several techniques. X-Ray Diffraction (XRD) was used for analysis of the purity and composition of the synthesized solid materials and performed on a Bruker D8 Advance X-ray diffractometer with Cu Kα radiation (λ = 1.5406 Å) and a LynxEye detector. All samples were prepared from powders except for the samples of the time-resolved investigation of the ferrihydrite transformation. These samples were prepared by drying small volumes of suspension directly on the XRD sample holder. XRD patterns of synthesized hematite were compared with hematite references (ICDD PDF-2 database) and showed that pure hematite was formed at 50°C without any evidences of contamination by goethite or other crystalline Fe oxides. For synthesized ferrihydrite, the XRD analysis revealed the formation of the most poorly crystalline ferrihydrite form, the 2-line ferrihydrite, which is identifiable by 2 broad peaks in the XRD plot with maxima at 2θ of ~35° and ~62° (Cu Kα).

BET measurements (Brunauer et al., 1938) were conducted on selected hematite and ferrihydrite samples using a Quantachrome Autosorb 1-MP and 11-point BET-argon isotherms recorded at the temperature of liquid argon (87.3K) to calculate the specific surface areas (SSA). Prior to the measurement, the sample were outgassed in vacuum at 95°C overnight to remove water and other volatile surface contaminations. The measurements gave a specific surface area of 65 m²/g for pure hematite and of 243 m²/g for pure ferrihydrite. The value of ferrihydrite is in good agreement with the given BET results of 200-320 m²/g for 2-line ferrihydrite of Schwertmann and Cornell (2000), whereas the values for hematite are significantly higher than their published data (20-25 m²/g). This difference can be explained by the lower synthesis temperature of 50°C compared to the original suggested 90°C, which results in smaller particle sizes of the hematite crystals (see below?).

The total Se content of the solid phases was determined by polarized Energy Dispersive X-ray Fluorescence Spectroscopy (pEDXRF) using an Epsilon 5 (PANalytical) equipped with a W X-ray tube and a Ge detector. A Mo target was selected as polarizing secondary target and the measurement period was 500 s. Standards consisting of mixtures of synthesized hematite and known amounts of a Se reference material (pure Se(0) powder or certified Se reference solution) were utilized for calibration.

Scanning Electron Microscopy with Energy Dispersive X-ray Spectroscopy (SEM/EDX) was used to characterize the morphology of the solid phases and to assess the size of the particles. Images were recorded using a LEO 1530 (Zeiss Inc.) SEM with a NORAN System SIX

(Thermo Electron Corp.) EDX-System. The dried powder samples were coated with Pt after they were mounted on sample holders via double-sided carbon tape. The optical characterization of the pure synthesis product revealed that hematite consists of aggregated bulky particles with a size of 50 to 100 nm (cf. chapter 3.3)

In order to examine the Se oxidation state and to identify ionic species on the hematite surface, X-ray Photoelectron Spectroscopy (XPS) measurements were performed using a PHI 5000 VersaProbe II (ULVAC-PHI Inc.). The system was equipped with a scanning microprobe X-ray source (monochromatic Al Kα, 1486.7 eV) in combination with an electron flood gun and a floating ion gun generating low-energy electrons (1.1 eV) and low energy argon ions (8 eV) for charge compensation at isolating samples (dual beam technique), respectively. Calibration of the binding energy scale of the spectrometer was performed using the well-established binding energies of elemental lines of pure metals (monochromatic Al Kα: Cu $2p_{3/2}$ at 932.62 eV, Au $4f_{7/2}$ at 83.96 eV, (Seah et al., 1998)). O1s (α-Fe_2O_3) at 529.6 eV was used as charge reference for the hematite samples (Moulder et al., 1995). Error of binding energies of elemental lines is estimated to ± 0.2 eV. Data analysis was performed using ULVAC-PHI MultiPak program, version 9.6. By means of XPS analysis (cf. chapter 3.4), it was possible to characterize the sorbed surface species and the chemical composition of unwashed hematite samples. As expected, higher amounts of C and lower amounts of N, K and Na can be found beside Fe and O in the region near the hematite surface mainly caused by adsorption of carbonate species ($NaHCO_3$ buffer) or nitrate. In addition, smaller amounts of precipitated K and Na salts cannot be completely excluded in case of unwashed samples.

X-ray Absorption Spectroscopy (XAS) analysis was carried out on selected samples to identify the Se oxidation state as well as the type and nature of bonding environment between Se and the iron oxide phases. The examination of hematite and ferrihydrite samples from coprecipitation, adsorption and desorption studies allowed for a detailled characterization of the Se retention mechanisms and provided information on the identification of Se incorporation processes. Se K-edge X-ray Absorption Near-Edge Structure (XANES) and Extended X-ray Absorption Fine-Structure (EXAFS) spectra were partly collected at the SUL-X beamline at ANKA (Karlsruhe, Germany), but mainly at the Rossendorf Beamline (ROBL) at ESRF (Grenoble, France).

At ANKA, Se K-edge XAS spectra were measured with a 7 element Si(Li) fluorescence detector. An elemental Se pellet (K-edge at 12658 eV) was used for calibration of the monochromator energy. For sample preparation, defined amounts of hematite or ferrihydrite

powder were mixed with cellulose and pressed into pellets. All spectra were collected at room temperature under normal atmospheric conditions.

For XAS analysis at ROBL, a 13 element high-purity germanium detector (Canberra) with digital signal processing (XIA) for fluorescence detection was used. The monochromator energy was calibrated with a gold foil (K-edge at 11919 eV) because of its greater inertness and hence reliability in comparison to elemental Se. During the sample preparation, small amounts of Se-bearing hematite and ferrihydrite powders were placed in sample holders and sealed with Kapton® tape. Spectra were collected at 15 K using a closed cycle He cryostat with a large fluorescence exit window and a low vibration level (CryoVac) in order to avoid photon-induced redox reactions. Dead time correction of the fluorescence signal, energy calibration and the averaging of single scans were performed with the software package SixPack. Normalization, transformation from energy into k space, and subtraction of a spline background was performed with WinXAS using routine procedures (Ressler, 1998). The k^3-weighted EXAFS data were fit with WinXAS using theoretical back-scattering amplitudes and phase shifts calculated with FEFF 8.2 (Ankudinov and Rehr, 1997). Statistical analysis of spectra was performed with the ITFA program package (Rossberg et al., 2003). Spectra of Se reference samples (crystalline Na_2SeO_4 and a Se(IV) solution) were taken from Scheinost and Charlet (2008).

2.7 Se sorption - Data analysis

Uptake of Se(IV) and Se(VI) by adsorption and coprecipitation was evaluated as proportion of the initial Se concentration (Se removal in %) or in form of the distribution coefficients (R_d), which considers the influence of the m/V ratio between the solid mass (hematite) and the volume of the aqueous solution. The R_d-value (L/kg) is defined as

$$R_d = \left(\frac{[Se]_{ini}}{[Se]_{eq}} - 1 \right) \cdot \frac{V}{m}$$

where $[Se]_{ini}$ is the total initial Se concentration (mol/L), $[Se]_{eq}$ the aqueous Se concentration at equilibrium (mol/L), V the total volume (L) of the aqueous solution and m the mass of hematite (kg).

3   Results and Discussion

3.1   Interaction of dissolved Se with hematite

3.1.1   Adsorption of Se(IV) and Se(VI) on hematite

The hematite adsorption capacity for Se(IV) and Se(VI) as a function of pH is shown in Fig. 1. These results are an essential basis for the evaluation and interpretation of the Se coprecipitation data and demonstrate that the adsorption behavior of Se(IV) and Se(VI) species is completely different. Hematite shows a strong adsorption for Se(IV) over a large pH range (pH 2-9), which is even significant at alkaline conditions above pH 10. In contrast, Se(VI) adsorption only takes place at acidic pH. Furthermore, the adsorption of Se(IV) is not influenced by the ionic strength, whereas the adsorption edge of Se(VI) is clearly shifted towards lower pH values (approx. 1 pH unit) in the presence of higher concentrations of competing NO_3^- anions. Fig. 1. also presents data (R_d) of Se(IV) and Se(VI) adsorption onto hematite as a function of the Se equilibrium concentration. At the constant pH of 7.5, adsorption of Se(IV) is extremely high even at very high equilibrium Se concentrations. Similar to the data of the pH study, the results also indicate that adsorption of Se(IV) is not affected by increasing ionic strength and that both Se(IV) data sets follow a clear trend. In contrast, adsorption of Se(VI) onto hematite is only weakly pronounced. Although the distribution coefficient of Se(VI) also follows a decreasing trend as long as no competing anions are present, the general level is much lower. In case of higher ionic strengths, adsorption of Se(VI) is almost non-existing under the investigated hydrochemical conditions.

The Se(IV)/Se(VI) adsorption behavior observed is consistent with data in previous studies by Duc et al. (2006) and Rovira et al. (2008) and suggest that adsorption of Se(IV) onto hematite can be attributed to a specific adsorption and the formation of inner-sphere surface complexes. Furthermore, the low Se(VI) adsorption to hematite and the strong negative impact of an increasing pH and ionic strength is constant with data of Se(VI) adsorption studies on other ferric oxide minerals (Su and Suarez, 2000; Rietra et al., 2001; Wijnja and Schulthess, 2002; Duc et al., 2003; Das et al., 2013).

3.1.2   Se(IV) and Se(VI) coprecipitation with hematite

Determining the residual Se concentration in solution after the coprecipitation experiments allowed the quantification of the Se(IV) or Se(VI) uptake during the hematite formation. Fig. 2 shows a comparison of the Se uptake by coprecipitation and adsorption as a function of the

Se equilibrium concentration at pH 7.5. Similar to the former adsorption results, Se(IV) and Se(VI) sorption during coprecipitation with hematite strongly depends on the Se speciation. The Se(IV) uptake by coprecipitation is extremely high and rises to values of more than 0.8 mol/kg, whereas the sorption of Se(VI) is limited over the entire concentration range (<0.05 mol/kg), cf. **Error! Reference source not found.**. Regarding the distinction between Se coprecipitation and adsorption, it is not possible to see clear differences in case of the Se(VI) data, due to the extremely low Se(VI) sorption capacity of hematite at neutral pH conditions. However, differences are clearly visible for the Se(IV) system in form of a significantly higher Se uptake by coprecipitation than by adsorption. While adsorption of Se(IV) reaches an upper limit at 0.2 - 0.3 mol/kg, the Se(IV) uptake by coprecipitation increases steadily without indications of a sorption limit. This difference in the uptake behavior between the adsorption and the coprecipitation experiments suggests a different uptake mechanism in both cases.

3.1.3 Se(IV) and Se(VI) desorption - Stability of the Se retention

In a first approach, the reversibility of Se uptake in the adsorption and coprecipitation samples was investigated by taking advantage of the low adsorption capacity of hematite at pH 12 (Fig. 1). Therefore, hematite samples from the Se adsorption and coprecipitation experiments, which were performed at 2 different initial Se concentrations of 10^{-4} mol/L and 10^{-3} mol/L, were treated with a desorption solution of pH 12 and the fraction of desorbed Se was determined by analyzing the amount of released Se (Fig. 3). The results show the known different behavior of Se(IV) and Se(VI) during the sorption step (bar heights), but also reveal that for both Se(IV) and Se(VI) the amount of desorbed Se is significantly higher for the sorption in contrast to the coprecipitation samples (Fig. 3 left). This behavior is also observed for the higher Se loading (Fig. 3 right). For all sorption samples, the treatment with the desorption solution causes the release of most of the adsorbed Se(IV) or Se(VI). In case of Se(IV), the release is equivalent to the hematite adsorption capacity at pH 12 (desorption of 80 - 90 %). Compared with this, less than 30 % of the taken up Se(IV) or Se(VI) is desorbed in case of the coprecipitated hematite samples.

The effect of OH^- concentration (or pH) on the stability of the Se retention was examined in detail for selected coprecipitation and adsorption samples of the Se(IV) system, as these samples showed major differences in their behavior not only in the desorption experiment but also during the actual Se sorption step. Fig. 4 shows the results of this study, which contains, beside different types of Se(IV)-bearing hematite samples, also a sample of a Se(IV)

coprecipitation with the hematite precursor ferrihydrite. In general, these results confirm the previous observation that the desorption behavior between coprecipitated and adsorbed hematite samples is completely different. Although the first release of Se(IV) starts at comparable OH$^-$ concentrations of about 10^{-4} mol/L ($\approx$ pH 10) for both types of sorption processes, the proportion of desorbed Se(IV) increases rapidly for the adsorbed hematite samples and reaches a total amount of about 80 % at the highest OH$^-$ concentration of 0.5 mol/L ($\approx$ pH 13.7). In contrast, the coprecipitated hematite samples show a slow increase of the desorbed Se fraction with an overall proportion of only about 20 % at the final stage. This is consistent with the results of the previous simple leaching studies at pH 12, particularly considering the 3-fold desorption in those experiments. Furthermore, the comparison between ferrihydrite and hematite reveals that the desorption behavior of ferrihydrite is similar to that of the hematite adsorption samples. This suggests that the interaction between Se(IV) and ferrihydrite remains adsorption rather than incorporation at this early stage of the coprecipitation process. However, a comparison of the total Se and Fe release (Fig. x in supplementary information) demonstrates that OH$^-$ concentrations of 0.5 mol/L are too low to dissolve significant amounts of the hematite phase ([Fe]/[Fe]$_{tot}$ max. $2 \cdot 10^{-3}$). A release of potentially incorporated Se(IV) can therefore be excluded.

Based on these desorption studies, it can be concluded that Se retention by coprecipitation with hematite is not only the predominant but also the more stable immobilization process compared to adsorption. This also suggests that the formation pathway of hematite has a significant influence on the interaction between dissolved Se oxyanions and the forming iron oxide.

3.2   Interaction of Se with the precursor ferrihydrite

Poorly crystalline 2-line ferrihydrite occurs as a metastable precursor of hematite that immediately precipitates from solution after the first increase of pH by adding KOH to the dissolved Fe^{3+}. Subsequently, the ferrihydrite phase progressively transforms into well crystalline hematite during the total reaction period of 10 days. The progress of this transformation process can be identified in the XRD plot by the time-dependent disappearance of the 2 broad ferrihydrite peaks with maxima at 2θ of ~35° and ~62°, which are associated with 2-line ferrihydrite (Fig. 5). Three selected Se(IV) coprecipitation samples show that the broad ferrihydrite peaks are visible in addition to the much stronger hematite lines after one and four days, while they have disappeared after 10 days and only those of hematite are left (main peaks at 2θ of ~24.1°, ~33.2°, ~35.6°, ~40.9°, ~49.5°, ~54.1°, ~62.5°,

14

~64.0°). This illustrates, that the transformation of ferrihydrite into hematite lasts a few days, during which the dissolved Se oxyanions interact with the crystallising phase. Note also the presence of precipitated background electrolyte KNO_3 (main peaks at 2θ of ~19.0°, ~23.6°, ~29.4°, ~32.4°, ~33.8° ~41.2°, ~43.7°, ~44.1°, ~46.6°) in all analyzed samples because of the sample drying without prior washing of the suspensions.

Fig. 6. shows the temporal evolution of the Se(IV) or Se(VI) concentrations in solution during the formation and transformation of ferrihydrite. In case of Se(IV), the fast precipitation of ferrihydrite leads to an immediate Se removal from solution. After titration to pH 7.5 (formation step 4) almost the entire initial Se amount is removed from solution, without any further changes within the subsequent 10 days during the ferrihydrite to hematite transformation. The behavior of Se(VI) is very different in so far as Se is removed from solution to below 20 % only at the time of the first ferrihydrite precipitation (formation step 2.), but then solution concentration increases rapidly to its final value of more than 90 %, where it remains unchanged for 10 days. This behavior, including the fast removal by ferrihydrite at low pH (about 2) and release with increasing pH is in line with the typical pH dependence of oxyanion outersphere sorption already documented in Fig. 1 (left). As tested in own preliminary studies and also described in the literature by several authors, Se shows a rapid adsorption kinetic on iron oxide minerals (Zhang and Sparks, 1990; Su and Suarez, 2000; Rovira et al., 2008; Mitchell et al., 2013). Again, this suggests that the uptake of Se(IV) in the coprecipitation experiments is different from adsorption and is ultimately by the ferrihydrite/hematite recrystallization.

3.3 Effect of the Se concentration on the type of Fe precipitates

Error! Reference source not found. compiles the main properties of some selected synthesized iron oxide samples from coprecipitation experiments with different initial Se concentrations. The data show that the proportion of sorbed Se is low for all coprecipitation samples of the Se(VI) system, but also that the presence of even extremely high Se(VI) concentrations has no effect on the formation of pure hematite and on the final pH. In the Se(IV) system, however, the coprecipitation causes a high Se retention, while at the same time higher concentrations of dissolved Se(IV) lead to an incomplete formation of hematite and instead to hematite-goethite mixed phases. In addition, high initial Se(IV) amounts cause an increase of the solution pH. This effect is visible at initial Se concentrations of more than 10^{-3} mol/L, and thus only when a certain Se/Fe ratio, or a certain Se content of the iron oxide phase, are exceeded. For the type of hematite synthesized in this study, this specific Se

content is in the range of about 0.7 - 1.3 wt%, which corresponds to the point in the sorption data where the retention ability of hematite for Se(IV) starts to decrease (Fig. 2). In contrast, the examination on ferrihydrite samples provide no evidence that a presence of higher amounts of Se(IV) affect the purity or composition of formed ferrihydrite. This means that the presence of Se during the crystallization of hematite from ferrihydrite has not only an impact on the Se retention process but equally influences the transformation process of ferrihydrite into hematite. This latter point is, however, only detectable in case of an exceedance of a certain Se concentration threshold as well as a strong interaction between the dissolved Se and the ferrihydrite/hematite phase, which occurs only for Se(IV). A similar inhibition of the ferrihydrite recrystallization by oxyanions species was reported, among others, by Gálvez et al. (1999a). There, a small amount of phosphate favored the transformation of ferrihydrite into hematite, whereas higher phosphate concentrations caused the formation of goethite. This behavior was attributed to the formation of inner-sphere adsorption complexes, which disturb the transformation of ferrihydrite into hematite due to the increasing negative surface charge at high phosphate concentrations. This is consistent with our data, where Se(IV) supposedly also interacts as an inner-sphere sorbed species with ferrihydrite or hematite.

Samples of the Se(VI) ferrihydrite system, on the other hand, show a behavior that is largely in accordance with the Se retention of the hematite system. At neutral pH conditions, the sorption behavior of ferrihydrite for Se(VI) is also clearly limited compared to the retention capacity for Se(IV), but the interaction does not affect the solid phases.

Table 1. Equilibrium (residual) concentrations of Fe and Se, the resulting Se removal (in % and log R_d) and the mineral composition (Hm: hematite, Gt: goethite, Fh: ferrihydrite) of selected samples of coprecipitation experiments with different initial amounts of Se; $^{"X"}$ $c(Se)_{ini}$ = "X" $\cdot$ 10^{-3} mol/L.

#	Se species	Sample	Mineral(s) [a]	Se [b] [ppm]	pH [c]	$c(Fe)_{eq}$ [mol/L]	$c(Se)_{ini}$ [mol/L]	$c(Se)_{eq}$ [mol/L]	Se sorbed [%]	log R_d [L/kg]
1	---	Hm (pure)	Hm	bdl	7.3	1.44E-07	0.00	bdl	---	---
2	Se(VI)	Se(VI)CopHm$^{0.1}$	Hm	34	7.6	1.33E-07	1.02E-04	8.66E-05	15.3	1.30
3	"	Se(VI)CopHm^1	Hm	280	7.3	8.74E-08	1.02E-03	8.97E-04	12.3	1.19
4	"	Se(VI)CopHm^2	Hm	190	7.7	2.09E-07	2.04E-03	1.80E-03	11.9	1.17
5	"	Se(VI)CopHm^4	Hm	480	7.4	1.78E-05	4.09E-03	4.05E-03	0.9	0.02
6	"	Se(VI)CopHm^6	Hm	760	7.3	3.32E-05	6.13E-03	6.13E-03	0.0	---
7	"	Se(VI)CopHm^8	Hm	1100	7.3	3.38E-06	8.18E-03	8.07E-03	1.2	0.14
8	"	Se(VI)CopHm^{10}	Hm	1600	7.7	1.25E-05	1.02E-02	1.01E-02	1.0	0.04
9	Se(IV)	Se(IV)CopHm$^{0.1}$	Hm	770	7.7	6.16E-08	1.00E-04	1.07E-07	99.9	5.01
10	"	Se(IV)CopHm^1	Hm	6900	7.6	5.70E-07	1.00E-03	1.19E-06	99.9	4.97
11	"	Se(IV)CopHm^2	Hm + Gt	13000	7.9	7.99E-08	2.01E-03	8.41E-06	99.6	4.42
12	"	Se(IV)CopHm^4	Gt + Hm	21000	8.5	2.59E-06	4.02E-03	4.88E-04	87.9	2.90
13	"	Se(IV)CopHm^6	Gt + Hm	35000	8.5	9.33E-06	6.02E-03	1.05E-03	82.5	2.72

14	"	Se(IV)CopHm[8]	Gt + Hm	39000	8.6	6.00E-06	8.03E-03	1.78E-03	77.9	2.59
15	"	Se(IV)CopHm[10]	Gt + Hm	50000	8.3	1.45E-05	1.00E-02	2.10E-03	79.1	2.62
16	---	Fh (pure)	Fh	bdl	7.9	2.74E-06	0.00	bdl	---	---
17	Se(VI)	Se(VI)CopFh[1]	Fh	1500	7.6	1.19E-05	1.02E-03	9.31E-04	8.9	4.34
18	"	Se(VI)CopFh[4]	Fh	6200	7.9	7.21E-06	4.09E-03	3.86E-03	5.5	1.04
19	Se(IV)	Se(IV)CopFh[1]	Fh	6200	8.1	7.42E-06	1.00E-03	5.07E-06	99.5	4.23
20	"	Se(IV)CopFh[4]	Fh	23000	8.1	3.72E-06	4.02E-03	2.57E-05	99.4	0.81

[a] Mineral compostion (XRD analysis). [b] Se content of the solid phase (EDXRF analysis). [c] pH after synthesis/coprecipitation

To what extent the interaction with Se affects the mineral formation can also be seen in SEM images of coprecipitated samples (Fig. 7). For initial Se amounts of $4 \cdot 10^{-3}$ mol/L, it is clearly visible that coprecipitation with Se(VI) produces only pure hematite (Fig. 7a), whereas coprecipitation with Se(IV) causes the formation of a goethite-hematite mixed phase (Fig. 7c). Furthermore, SEM analysis of comparable hematite adsorption samples indicate that neither adsorption of Se(VI) nor Se(IV) has an influence on the hematite phase (Fig. 7b,d). This behavior was also verified by XRD results of hematite samples from adsorption studies (not shown).

3.4 Spectroscopic characterization of the retention mechanisms

The XPS-determined elemental composition on the iron oxide surface as well as selcetd oxidation states are shown in Table 2. The data prove that for samples of the Se(IV) system (prepared of an initial Se(IV) source), the sorbed Se in the near-surface area of hematite occurs in the oxidation state Se(IV) in both analyzed coprecipitation and adsorption samples. The interaction processes between dissolved Se(IV) and hematite consequently cause no changes of the Se(IV) valency. Note that for the Se-bearing hematite samples of the Se(VI) system, Se uptake was too low to determine the oxidation state by XPS, even for samples with high initial Se concentrations of $8 \cdot 10^{-3}$ mol/L.

Table 2. XPS results of hematite samples (unwashed): Atomic concentrations (at%) of main elements and Se binding energies (eV) of several spectral lines for Se(IV)-bearing samples.

Sample	C	N	O	Na	K	Fe	Se
Hm (pure)	14.3	1.2	54.8	0.3	1.9	27.5	---
Se(VI)CopHm[8]	13.8	0.6	54.4	1.0	0.8	29.3	traces
Se(VI)AdsHm[8]	14.8	0.8	55.3	---	0.7	28.4	traces
Se(IV)CopHm[1]	4.3	1.4	60.3	0.9	2.5	30.4	0.3
Se(IV)AdsHm[1]	12.9	1.3	56.0	---	0.9	28.1	0.8

Atomic concentrations: relative error ± 10-20 %

Sample	Se 3s	Se L$_3$M$_{45}$M$_{45}$	Se 3p$_{3/2}$	Se L$_2$M$_{45}$M$_{45}$	O 1s	(charge ref.)	Se valency
Se(IV)CopHm[1]	233.6	185.1	164.7	143.7	529.6	α-Fe$_2$O$_3$	Se(IV)

| Se(IV)AdsHm[1] | 233.5 | 185.2 | 164.8 | 143.8 | 529.6 | α-Fe₂O₃ | Se(IV) |

Binding energy: error ± 0.2 eV

Further analysis of the (bulk) Se oxidation state was performed via XANES. All collected Se K-edge XANES spectra of Se-bearing hematite and ferrihydrite samples show strong white lines, which occur at identical positions for all samples within the same system, at 12.663 keV for Se(VI), and at 12.660 keV for Se(IV) (Fig. 8). Both values match the white line positions of Se reference spectra (Na$_2$SeO$_4$: 12.663 keV, Se(IV) ref. solution: 12.660 keV) and indicate that the Se oxidation state remained unaltered by the reaction with hematite or ferrihydrite.

In order to characterize the Se retention mechanisms in detail, samples of each system with different natures of Se sorption - partly more than one of the same type - were analyzed by Se K-edge EXAFS spectroscopy (Fig. 8). The k^3-weighted χ spectra were fit with a FEFF 8.2 file that was generated with the crystallographic structure of mandarinoite (Fe$_2$(SeO$_3$)$_3$·6H$_2$O, CIF 0005198, Hawthorne, 1984). For all samples of the Se(VI) system, the EXAFS Fourier transform magnitude is dominated by strong peaks at 1.3 Å (uncorrected for phase shift), which result from oxygen atoms in the coordination shell. A fit of this peak with a single scattering Se-O path lead to coordination numbers (CN) for the oxygen atoms of 3.3 - 3.8 and to atomic distances of 1.65 Å (Table 3), confirming the unchanged hexavalent oxidation state and the tetrahedral structure of the Se(VI) anion. Apart from that, no additional peaks are visible and thus no signs of further shells beyond the oxygen coordination sphere. This indicates the presence of a hydration sphere and hence outer-sphere bonding of the Se(VI) species for all analyzed iron oxides. No indication for inner-sphere sorption or any evidence of incorporation was found. Concluding from a number of previous studies about Se(VI) adsorption on goethite, Se(VI) species are able to form both inner- and outer-sphere adsorption complexes depending on the respective conditions. While some authors solely identified inner-sphere Se(VI) complexes on goethite (Su and Suarez, 2000; Das et al., 2013), other publications demonstrated the formation of a mixture of inner- and outer-sphere adsorption complexes, whereby the distribution of both types strongly depends on parameters like pH, ionic strength or the surface coverage (Peak and Sparks, 2002; Fukushi and Sverjensky, 2007). Especially the pH plays a key role in this context and leads, at least in case of goethite, to the formation of mainly inner-sphere complexes at pH values below 6, whereas a higher pH causes the formation of primarily outer-sphere complexes (Rietra et al., 2001; Wijnja and Schulthess, 2002). In contrast, the interaction of Se(VI) with hematite and ferrihydrite is not so well studied and partly contradictory in terms of the nature of the Se(VI)

complexes. According to Peak and Sparks (2002), the behavior of ferrihydrite should be similar to that of goethite, which is consistent with our results when taking into account the neutral pH conditions and the mentioned pH dependency. The hydrochemical conditions during the mineral synthesis are responsible for a relatively high ionic strength, which would favor innersphere sorption because of competition effects; however, this was not observed. Our results are hence in disagreement with those of Das et al. (2013), who clearly identified inner-sphere Se(VI) complexes on ferrihydrite at comparable neutral pH conditions, but at substantially lower ionic strengths. Published data of Se(VI) adsorption on hematite (Peak and Sparks, 2002) demonstrate an inner-spheric complexation, which is additionally unaffected by pH. A possible reason for this difference could be the dominant anion in the used background electrolyte (here nitrate instead of chloride). While chloride is known to have one the lowest adsorption affinities for iron oxides, the affinity of the oxyanion nitrate is higher and more comparable with selenate (Neal, 1995), hence nitrate most likely out-competes selenate at innersphere sorption sites.

For the samples of the Se(IV) system, the EXAFS Fourier transform show the oxygen coordination shell at about 1.4 Å (uncorrected for phase shift, Fig. 8). A fit of those peaks result in coordination numbers of 2.7 - 3.0 and atomic distances of 1.70 - 1.71 Å (Table 3), confirming the tetravalent Se oxidation state. This means when Se(IV) is used as the initial Se species, its pyramidal-shaped structure (Chen et al., 1999) and coordination by 3 oxygen atoms remains unchanged even after the interaction with iron oxides.

In contrast to the Se(VI) system, the Fourier transform of the EXAFS spectra of Se(IV) samples show further structural features beyond the oxygen coordination shell. Two peaks that appear close to each other rise above the background in the range at 2.5 - 3.0 Å (uncorrected for phase shift), whereby the signal intensity, the form and the distances of those peaks differ in dependency of the sample origin and the associated Se sorption type. Two individual single scattering Se-Fe paths were used to achieve a good fitting of those peaks (Table 3), whereas the use of only one Se-Fe path or a mixture of Se-Fe and Se-O paths led to poor results. Note that the Debye-Waller factors of both Se-Fe paths were kept correlated to obtain stable fit results. In general, the presence of Fe atoms in the second shell implies a direct linkage of the Se(IV) oxyanions to the iron oxide without an additional hydration sphere and thus a bonding of an inner-spheric nature.

Table 3. Se-K XANES edge energies and EXAFS fit results of hematite and ferrihydrite samples ($S_0^2 = 0.9$).

	oxygen shell			iron shells	

Sample	E_0 [keV]	CN^a		R [Å]^b	σ^2 [Å²]^c	CN		R [Å]	σ^2 [Å²]		ΔE_0 [eV]	χ_{res} [%]
Se(VI)CopHm[10]	12.6629	3.3	O	1.65	0.0020						14.5	8.1
Se(VI)CopFh[4]	12.6632	3.6	O	1.65	0.0009						14.8	8.2
Se(VI)AdsHm[8]	12.6633	3.6	O	1.65	0.0013						14.4	9.3
Se(VI)AdsHm[4]	12.6632	3.6	O	1.66	0.0004						15.5	9.5
Se(VI)AdsHm[1]-pH4	12.6632	3.8	O	1.65	0.0010						14.8	8.0
Se(IV)CopHm[1]	12.6597	2.9	O	1.71	0.0015	0.7	Fe	2.94	0.0097	#	15.2	13.8
						2.5	Fe	3.43	0.0097	#		
Se(IV)CopHm[1]	12.6596	3.0	O	1.71	0.0015	0.5	Fe	2.95	0.0100	#,§	15.8	14.1
						2.4	Fe	3.41	0.0100	#,§		
Se(IV)CopHm[1]-DeSo	12.6595	3.0	O	1.71	0.0014	0.9	Fe	2.98	0.0100	#,§	15.5	13.9
						2.8	Fe	3.43	0.0100	#,§		
Se(IV)CopFh[1]	12.6595	2.9	O	1.70	0.0014	0.3	Fe	2.89	0.0100	#,§	15.3	14.4
						1.4	Fe	3.34	0.0100	#,§		
Se(IV)CopFh[4]	12.6595	2.8	O	1.71	0.0013	0.3	Fe	2.88	0.0072	#	15.6	12.8
						1.1	Fe	3.34	0.0072	#		
Se(IV)AdsHm[1]	12.6596	2.9	O	1.71	0.0016	0.3	Fe	2.90	0.0056	#	15.5	13.1
						1.6	Fe	3.38	0.0056	#		
Se(IV)AdsHm[4]	12.6598	2.9	O	1.70	0.0018	0.3	Fe	2.89	0.0049	#	15.1	12.1
						1.3	Fe	3.37	0.0049	#		
Se(IV)AdsHm[1]-pH4	12.6594	2.7	O	1.70	0.0011	0.4	Fe	2.91	0.0030	#	15.5	12.8
						0.8	Fe	3.38	0.0030	#		

^{a} CN: coordination number, error ± 25%. ^{b} R: Radial distance, error ± 0.01 Å. ^{c} σ²: Debye-Waller factor, error ± 0.0005 Å².
$^#$ correlated σ². § Upper σ² limit reached. $^{"X"}$ c(Se)$_{ini}$ = "X" · 10^{-3} mol/L. "DeSo": Sample from desorption studie.

These fit results, which include the first published EXAFS fittings of Se(IV) interaction with hematite, are in good agreement with published data of Se(IV) adsorption on other types of iron (oxyhydr)oxides, particularly in terms of the atomic Fe distances of 2.88 - 2.98 Å for the shorter-distant and 3.34 - 3.43 Å for the longer-distant Fe atoms. These distances suggest the formation of a bidentate mononuclear edge-sharing ^{1}E arrangement between the SeO_3^{2-} pyramidal molecule and the hematite FeO_6 octahedra in case of the shorter-distant Fe atoms, while the longer-distant Fe shell represents bidentate binuclear corner-sharing ^{2}C complexes (Hayes et al., 1987; Manceau and Charlet, 1994; Hiemstra et al., 2007; Missana et al., 2009; Jordan et al., 2014). Both types of complexes occur in all investigated hematite and ferrihydrite samples at the same time, and were also observed for ferrihydrite (Manceau and Charlet, 1994), magnetite (Missana et al., 2009) and maghemite (Jordan et al., 2013; Jordan et al., 2014). The only iron oxyhydroxide mineral with different adsorption characteristics is goethite, for which, by EXAFS or IR spectrometry, only corner-sharing ^{2}C complexes were identified (Hayes et al., 1987; Manceau and Charlet, 1994; Su and Suarez, 2000). The formation of corner- and edge-shared complexes on specific crystal surfaces and their proportions depends on pH (Jordan et al., 2013; Jordan et al., 2014), crystal morphology (Manceau and Charlet, 1994), and, in particular, the surface coverage, whereby higher coverages favor the formation of both corner- and edge-shared complexes (Missana et al., 2009). This would explain why all investigated Se(IV)-bearing hematite and ferrihydrite

samples show both types of surface complexes, since they all have higher surface coverages as well as no preferred orientation compared to generally needle-shaped goethite crystals.

The key finding of the fitting is, however, that all hematite samples, which have the theoretical possibility of an incorporated Se(IV) fraction, show significantly higher coordination numbers and also larger Se-Fe distances than the hematite or ferrihydrite samples where incorporation of Se(IV) is very unlikely or can be ruled out by the sorption studies as shown above. This latter group includes hematite and ferrihydrite samples with only an adsorbed fraction of Se [Se(IV)AdsHm and Se(IV)CopFh], which are all characterized by smaller coordination numbers and distances of 0.3 - 0.4 at 2.88 - 2.91 Å for the short-distant Fe atoms and of 0.8 - 1.6 at 3.34 - 3.38 Å for the far-distant Fe shell. These coordination numbers fit very well with the assumed adsorption model, consisting of a mixture of mononuclear edge-sharing and binuclear corner-sharing inner-sphere complexes. In contrast, all hematite samples of coprecipitation experiments [Se(IV)CopHm], especially the afterwards desorbed one, show larger coordination numbers and distances of 0.5 - 0.9 at 2.94 - 2.98 Å for the shorter-distant Fe atoms and 2.4 - 2.8 at 3.41 - 3.43 Å for the longer-distant Fe atoms. Compared to the adsorbed samples, these coordination numbers, with values clearly above 2.0 in case of the far-distant Fe atom, are too high to be explained by the formation of typical surface adsorption complexes.

In order to verify and, at best, confirm the different characteristics of Se coprecipitation and adsorption, a statistical analysis of the EXAFS spectra was performed using Iterative Transformation Factor Analysis (ITFA) (Rossberg et al., 2003; Scheinost and Charlet, 2008). Fig. 9 (left) shows the excellent match between the experimental spectra (black lines) and their reconstructions (red lines) by two principal components (PC). The Principal Component Analysis reveals therefore that two different Se sorption species or mechanisms are needed to characterize the spectra of all Se(IV) samples. Furthermore, the Varimax factor loadings (Fig. 9, right) demonstrate that PC 1 is mainly present in the hematite samples of coprecipitation experiments, while the Se(IV) adsorption samples are dominated by PC 2. The statistical analysis therefore confirms the previous interpretation of the fitting results in terms that the retention mechanisms for Se coprecipitation and adsorption are different.

One possible explanation for the EXAFS results of the coprecipitated hematite samples would be the formation of an independent solid Se and Fe hosting mineral phase. Missana et al. (2009) reported that under certain circumstances, especially low pH values, sorption of Se(IV) onto magnetite can induce the precipitation of ferric selenite [$Fe_2(SeO_3)_3 \cdot 6\,H_2O$] as a

crystalline species. In a similar way, Bolanz et al. (2013) demonstrated for As(V) that an interaction during the ferrihydrite-hematite recrystallization causes the formation of angelellite-like clusters [$Fe_4As_2O_{11}$], which are incorporated in the hematite phase as a separate structural composite. However, both mineral structures would produce characteristic structural features in EXAFS FT region beyond 3 Å indicative of significant long-range order, which are absent in our samples; the formation of an independent Se and Fe containing mineral phase can hence be excluded for our study.

An alternative, and the more likely, explanation for higher coordination numbers than the expected ones for adsorption complexes (in our case higher than 0.5 and 1.0, respectively, for a spectral mixture of the two identified sorption complexes) are structural incorporation processes. However, the signal intensity and coordination numbers of the Fe are relatively low, and there is a lack of structural features beyond 3.5 Å (for uncorrected phase shift), which is rather untypical for a structural incorporation based on substitution or the occupation of crystallographic sites (vacancies). Moreover, such an incorporation of oxyanions into the hematite crystal lattice was proven practically only for P(V) (Gálvez et al., 1999b) and theoretically for Tc(VII) (Skomurski et al., 2010). Both P(V) and Tc(VII) have a tetrahedral structure and are coordinated by 4 oxygen atoms, which enables to occupy the tetrahedral vacancies within the hematite crystal structure. Since an occupation of the hematite tetrahedral or octahedral sites seems to be unrealistic in case of the pyramidal-shaped Se(IV), this indicates Se(IV) is incorporated in a different form. This incorporation mechanism is not characterized by an occupation of the hematite crystallographic sites but is also not an occlusion, due to the specific linkage between the Se(VI) molecules and the hematite. The incorporation process follows the prior Se(IV) adsorption onto ferrihydrite and takes place during the transformation of ferrihydrite into hematite, which is why the incorporated Se(IV) species are bound to the hematite phase in a way that is similar to Se(IV) inner-sphere adsorption complexes. A possible example for an analogous sorption mechanism was described by Scheinost et al. (2006) for Sb(V). In this case, EXAFS results provided indications of a comparable incorporation of Sb(V) into the structure of an iron oxide mineral. Just like Se(IV) in our results, this Sb(V) species showed two sorption complexes with associated coordination numbers that were larger than the expected ones of surface adsorption complexes, but were also too small to be explained by substitution or the occupation of vacancies.

The hypothesis of a Se incorporation mechanism is also supported by the general behavior of Se(VI). Although it is not possible to directly verify incorporation of Se(VI) into hematite by EXAFS data, on the basis of the hydrochemical sorption results, it can, nevertheless, be assumed that also Se(VI) gets incorporated into hematite during the ferrihydrite transformation. Especially the Se(VI) behavior in the aquatic phase and the stability of the Se(VI) retention against subsequent desorption (Fig. 3) are clear signs for the presence of an incorporated Se(VI) fraction. However, since this incorporated Se(VI) fraction is, according to the EXAFS data, still bound in form of outer-sphere complexes, a corresponding Se(VI) incorporation process is definitely not associated with a change of the surface complexation type. This supports the previous findings of the Se(IV) data evaluation, that incorporation of Se oxyanions into hematite cannot be attributed to substitution or occupation of crystallographic sites within the hematite lattice.
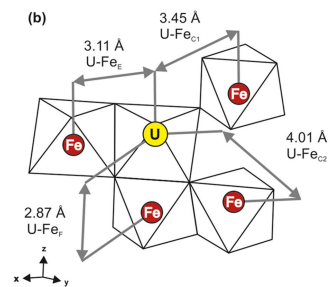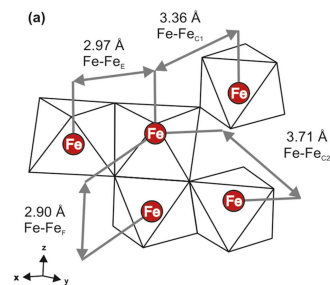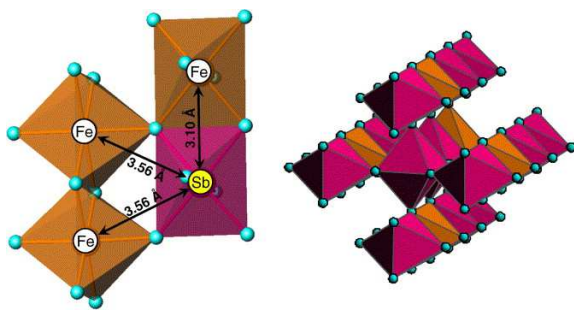
3.5 Conceptual model of the Se retention during the crystallization of hematite

The combination of hydrochemical and spectroscopic data of the solid phases lead to the outcome that three individual interaction processes control the fate of dissolved Se oxyanions during coprecipitation with hematite. The first process is the fast coprecipitation of Se oxyanions with ferrihydrite. Due to the large specific surface area of ferrihydrite, high quantities of Se can be adsorbed on the surface. The different surface areas of poorly crystalline ferrihydrite and well crystalline hematite are the reason why the uptake of Se resulting from coprecipitation is potentially higher than the Se uptake by pure adsorption on hematite after a completed mineral formation. The first adsorption of Se on ferrihydrite

23

therefore significantly defines the total amount of sorbed Se during the whole coprecipitation process. Since the ferrihydrite adsorption capacity for Se, like for all iron oxides, is strongly influenced by the Se speciation and the parameters pH and ionic strength, this interaction process is responsible for the much larger uptake of inner-sphere bound Se(IV) than of outer-sphere bound Se(VI), at least under the investigated conditions.

The second interaction process represents the incorporation of Se during the transformation of unstable ferrihydrite into crystalline hematite. The Se incorporation is less critical for the amount of sorbed Se, but is crucial for the stability of the Se retention, since the majority of adsorbed Se oxyanions are incorporated into the hematite during its crystallization. Coprecipitated Se, with a high fraction of incorporated Se, is thus more stable against a subsequent desorption than solely adsorbed Se oxyanions. In case of high Se concentrations and high adsorption, i.e. under neutral or alkaline pH conditions and for Se(IV), the surface coverage of ferrihydrite can become so high that the adsorbed Se complexes prevent a complete transformation of ferrihydrite into hematite. In this case, the transformation of ferrihydrite in hematite, which involves internal dehydration and rearrangement processes (Adegoke et al., 2013), seems to be no longer possible. Instead, the ferrihydrite transforms via dissolution and precipitation that causes the formation of goethite instead of hematite.

The last process, after the complete iron oxide formation, can be described as the general interaction between the solid hematite phase and all dissolved water components, including Se and competing anions, which leads to the adjustment of a Se adsorption/desorption equilibrium. The adsorption equilibrium of Se and hematite depends, similar to the previous Se adsorption on ferrihydrite, on the hydrochemical conditions and the hematite properties, as these parameters determine the type of possible adsorption complexes and therefore the amount of removable Se. But in case of former Se coprecipitation, this last step affects only the retention behavior and stability of the adsorbed Se fraction, which is, however, not that high, because most of the Se is already incorporated at that point and no longer in contact with the aquatic phase.

4 Conclusion

This study has demonstrated that during the crystallization of hematite from ferrihydrite under natural conditions, interacting Se oxyanions are not adsorbed but mainly incorporated into hematite. This incorporation process follows the previous adsorption of Se oxyanions onto ferrihydrite, the primarily precipitated iron oxide phase, and takes place during the subsequent

transformation of amorphous ferrihydrite into crystalline hematite. The proportion of incorporated Se is largely defined by the adsorption capacity of ferrihydrite for Se(IV) and Se(VI) under the prevailing conditions prior to the crystallization process. The incorporation mechanism itself is of a structural character and no occlusion, but is not attributed to substitution or occupation of crystallographic sites within the hematite crystal lattice. This is why the incorporated Se oxyanion species are bound to the hematite phase in a way that is similar to surface adsorption complexes – outer-sphere complexes for Se(VI) and inner-sphere complexes for Se(IV). Compared to adsorbed Se oxyanions, the retention of the incorporated Se fraction is very resistant even at alkaline pH conditions at least as long as the hematite mineral remains stable.

These results provide new knowledge about the retention behavior of Se oxyanions in natural environments. This concerns all places where iron oxides are newly formed or mineral transformation processes take place, including, for instance, the far-field of HLW disposal sites (interaction of [79]Se with secondary iron oxides) or the oxidized, near-surface regions of contaminated areas or within the critical zone. In all these environments, incorporation of Se oxyanions into iron oxides, and specifically hematite, can represent a main long-term immobilization mechanism. This may be important for mobility assessments of Se oxyanions or could be applied for the treatment of polluted wastewaters.

Acknowledgments

References

Adegoke H. I., Adekola F. A., Fatoki O. S. and Ximba B. J. (2013) Sorptive interaction of oxyanions

with iron oxides: A Review. *Polish J. Environ. Stud.* **22**, 7–24.

Ankudinov A. L. and Rehr J. J. (1997) Relativistic calculations of spin-dependent x-ray-absorption spectra. *Phys. Rev. B* **56**, 1712–1715.

Bajaj M., Eiche E., Neumann T., Winter J. and Gallert C. (2011) Hazardous concentrations of selenium in soil and groundwater in North-West India. *J. Hazard. Mater.* **189**, 640–646.

Balistrieri L. S. and Chao T. T. (1990) Adsorption of selenium by amorphous iron oxyhydroxide and manganese dioxide. *Geochim. Cosmochim. Acta* **54**, 739–751.

Bingham P. A., Connelly A. J., Cassingham N. J. and Hyatt N. C. (2011) Oxidation state and local environment of selenium in alkali borosilicate glasses for radioactive waste immobilisation. *J. Non. Cryst. Solids* **357**, 2726–2734.

Bolanz R. M., Wierzbicka-Wieczorek M., Čaplovičová M., Uhlík P., Göttlicher J., Steininger R. and Majzlan J. (2013) Structural Incorporation of As 5+ into Hematite. *Environ. Sci. Technol.* **47**, 9140–9147.

Brunauer S., Emmett P. H. and Teller E. (1938) Gases in Multimolecular Layers. *J. Am. Chem. Soc.* **60**, 309–319.

Cannière P. De, Maes A., Williams S., Bruggeman C., Beauwens T., Maes N. and Cowper M. (2010) *Behaviour of Selenium in Boom Clay. State-of-the-art report.*, SCK•CEN, Mol, Belgium.

Catalano J. G., Zhang Z., Fenter P. and Bedzyk M. J. (2006) Inner-sphere adsorption geometry of Se(IV) at the hematite (100)-water interface. *J. Colloid Interface Sci.* **297**, 665–671.

Chen F., Burns P. C. and Ewing R. C. (1999) 79Se: geochemical and crystallo-chemical retardation mechanisms. *J. Nucl. Mater.* **275**, 81–94.

Christophersen O. A., Lyons G., Haug A. and Steinnes E. (2012) Selenium. In *Heavy Metals in Soils: Trace Metals and Metalloids in Soils and their Bioavailability* (ed. B. J. Alloway). Springer, Dordrecht, NL. pp. 429–464.

Cornell R. M. and Schwertmann U. (2003) *The iron oxydes: Structure, Properties, Reactions, Occurences and Uses*. 2nd ed., Wiley-VCH, Weinheim, DE.

Das S., Hendry J. M. and Essilfie-Dughan J. (2013) Adsorption of selenate onto ferrihydrite, goethite, and lepidocrocite under neutral pH conditions. *Appl. Geochemistry* **28**, 185–193.

Dhillon K. S. and Dhillon S. K. (2003) Distribution and management of seleniferous soils. *Adv. Agron.* **79**, 119–184.

Doornbusch B., Bunney K., Gan B. K., Jones F. and Gräfe M. (2015) Iron oxide formation from FeCl2

solutions in the presence of uranyl (UO22+) cations and carbonate rich media. *Geochim. Cosmochim. Acta* **158**, 22–47.

Duc M., Lefèvre G. and Fédoroff M. (2006) Sorption of selenite ions on hematite. *J. Colloid Interface Sci.* **298**, 556–563.

Duc M., Lefèvre G., Fédoroff M., Jeanjean J., Rouchaud J. C., Monteil-Rivera F., Dumonceau J. and Milonjic S. (2003) Sorption of selenium anionic species on apatites and iron oxides from aqueous solutions. *J. Environ. Radioact.* **70**, 61–72.

Fernández-Martínez A. and Charlet L. (2009) Selenium environmental cycling and bioavailability: A structural chemist point of view. *Rev. Environ. Sci. Biotechnol.* **8**, 81–110.

Fukushi K. and Sverjensky D. A. (2007) A surface complexation model for sulfate and selenate on iron oxides consistent with spectroscopic and theoretical molecular evidence. *Geochim. Cosmochim. Acta* **71**, 1–24.

Gálvez N., Barrón V. and Torrent J. (1999a) Effect of phosphate on the crystallization of hematite, goethite, and lepidocrocite from ferrihydrite. *Clays Clay Miner.* **47**, 304–311.

Gálvez N., Barrón V. and Torrent J. (1999b) Preparation and Properties of Hematite with Structural Phosphorus. *Clays Clay Miner.* **47**, 375–385.

Grambow B. (2008) Mobile fission and activation products in nuclear waste disposal. *J. Contam. Hydrol.* **102**, 180–186.

Hawthorne F. C. (1984) The crystal structure of mandarinoite, Fe3+2Se3O9·6H2O. *Can. Mineral.* **22**, 475–480.

Hayes K. F., Roe A. L., Brown G. E., Hodgson K. O., Leckie J. O. and Parks G. A. (1987) In-Situ X-ray Absorption Study of Surface Complexes: Selenium Oxyanions on α-FeOOH. *Science (80-.).* **238**, 783–786.

Hiemstra T., Rietra R. P. J. J. and Van Riemsdijk W. H. (2007) Surface Complexation of Selenite on Goethite: MO/DFT Geometry and Charge Distribution. *Croat. Chem. Acta* **80**, 313–324.

Iida Y., Yamaguchi T., Tanaka T., Kitamura A. and Nakayama S. (2009) Determination of the solubility limiting solid of the selenium in the presence of iron under anoxic conditions. In *Mobile fission and activation products in nuclear waste disposal. Workshop Proceedings, La Baule, France, 16-19 January 2007.* OECD Nuclear Energy Agency. pp. 135–145.

Jordan N., Ritter A., Foerstendorf H., Scheinost A. C., Weiß S., Heim K., Grenzer J., Mücklich A. and Reuther H. (2013) Adsorption mechanism of selenium(VI) onto maghemite. *Geochim. Cosmochim. Acta* **103**, 63–75.

Jordan N., Ritter A., Scheinost A. C., Weiss S., Schild D. and Hübner R. (2014) Selenium(IV) uptake by maghemite (γ-Fe2O3). *Environ. Sci. Technol.* **48**, 1665–1674.

Lenz M. and Lens P. N. L. (2009) The essential toxin: The changing perception of selenium in environmental sciences. *Sci. Total Environ.* **407**, 3620–3633.

Liu J., Liang C., Zhang H., Tian Z. and Zhang S. (2012) General Strategy for Doping Impurities (Ge, Si, Mn, Sn, Ti) in Hematite Nanocrystals. *J. Phys. Chem.* **116**, 4986–4992.

Mallants D., Marivoet J. and Sillen X. (2001) Performance assessment of the disposal of vitried high-level waste in a clay layer. *J. Nucl. Mater.* **298**, 125–135.

Manceau A. and Charlet L. (1994) The Mechanism of Selenate Adsorption on Goethite and Hydrous Ferric Oxide. *J. Colloid Interface Sci.* **168**, 87–93.

Martínez M., Giménez J., de Pablo J., Rovira M. and Duro L. (2006) Sorption of selenium(IV) and selenium(VI) onto magnetite. *Appl. Surf. Sci.* **252**, 3767–3773.

Missana T., Alonso U., Scheinost A. C., Granizo N. and García-Gutiérrez M. (2009) Selenite retention by nanocrystalline magnetite: Role of adsorption, reduction and dissolution/co-precipitation processes. *Geochim. Cosmochim. Acta* **73**, 6205–6217.

Mitchell K., Couture R.-M., Johnson T. M., Mason P. R. D. and Van Cappellen P. (2013) Selenium sorption and isotope fractionation: Iron(III) oxides versus iron(II) sulfides. *Chem. Geol.* **342**, 21–28.

Moulder J. F., Stickle W. F., Sobol P. E. and Bomben K. D. (1995) *Handbook of X-ray Photoelectron Spectroscopy*. eds. J. Chastain and R. C. J. King, ULVAC-PHI, Inc. (Japan); Physical Electronics USA, Inc.

Neal R. H. (1995) Selenium. In *Heavy Metals in Soils* (ed. B. J. Alloway). Blackie Academic & Professional, London, UK. pp. 260–283.

Parida K. M., Gorai B., Das N. N. and Rao S. B. (1997) Studies on ferric oxide hydroxides - III. Adsorption of selenite (SeO32–) on different forms of iron oxyhydroxides. *J. Colloid Interface Sci.* **185**, 355–362.

Peak D. and Sparks D. L. (2002) Mechanisms of selenate adsorption on iron oxides and hydroxides. *Environ. Sci. Technol.* **36**, 1460–1466.

Ressler T. (1998) WinXAS: a program for X-ray absorption spectroscopy data analysis under MS-Windows. *J. Synchrotron Radiat.* **5**, 118–122.

Rietra R. P. J. J., Hiemstra T. and van Riemsdijk W. H. (2001) Comparison of Selenate and Sulfate Adsorption on Goethite. *J. Colloid Interface Sci.* **240**, 384–390.

Roh Y., Lee S. Y. and Elless M. P. (2000) Characterization of corrosion products in the permeable reactive barriers. *Environ. Geol.* **40**, 184–194.

Rossberg A., Reich T. and Bernhard G. (2003) Complexation of uranium(VI) with protocatechuic acid-application of iterative transformation factor analysis to EXAFS spectroscopy. *Anal. Bioanal. Chem.* **376**, 631–638.

Rovira M., Giménez J., Martínez M., Martínez-Lladó X., de Pablo J., Martí V. and Duro L. (2008) Sorption of selenium(IV) and selenium(VI) onto natural iron oxides: Goethite and hematite. *J. Hazard. Mater.* **150**, 279–284.

Scheinost A. C. and Charlet L. (2008) Selenite reduction by mackinawite, magnetite and siderite: XAS characterization of nanosized redox products. *Environ. Sci. Technol.* **42**, 1984–1989.

Scheinost A. C., Rossberg A., Vantelon D., Xifra I., Kretzschmar R., Leuz A. K., Funke H. and Johnson C. A. (2006) Quantitative antimony speciation in shooting-range soils by EXAFS spectroscopy. *Geochim. Cosmochim. Acta* **70**, 3299–3312.

Schwertmann U. and Cornell R. M. (2000) *Iron oxides in the laboratory: Preparation and characterization*. 2nd, compl., Wiley-VCH, Weinheim.

Seah M. P., Gilmore I. S. and Beamson G. (1998) XPS: Binding Energy Calibration of Electron Spectrometers 5 - Re-evaluation of the Reference Energies. *Surf. Interface Anal.* **26**, 642–649.

Séby F., Potin-Gautier M., Giffaut E., Borge G. and Donard O. F. X. (2001) A critical review of thermodynamic data for selenium species at 25°C. *Chem. Geol.* **171**, 173–194.

Séby F., Potin-Gautier M., Giffaut E. and Donard O. F. X. (1998) Review Assessing the speciation and the biogeochemical processes affecting the mobility of selenium from a geological repository of radioactive wastes to the biosphere. *Analusis* **26**, 193–198.

Skomurski F. N., Rosso K. M., Krupka K. M. and McGrail B. P. (2010) Technetium Incorporation into Hematite (a-Fe2O3). *Environ. Sci. Technol.* **44**, 5855–5861.

Soltis J. A., Feinberg J. M., Gilbert B. and Penn R. L. (2016) Phase Transformation and Particle-Mediated Growth in the Formation of Hematite from 2-Line Ferrihydrite. *Cryst. Growth Des.* **16**, 922–932.

Sparks D. L. (2003) *Environmental Soil Chemistry*. 2nd ed., Academic Press, Amsterdam, NL.

Sracek O. (2015) Formation of secondary hematite and its role in attenuation of contaminants at mine tailings: review and comparison of sites in Zambia and Namibia. *Front. Environ. Sci.* **2**, 1–11.

Su C. and Suarez D. L. (2000) Selenate and Selenite Sorption on Iron Oxides. *Soil Sci. Soc. Am. J.* **64**, 101–111.

Wijnja H. and Schulthess C. P. (2002) Effect of Carbonate on the Adsorption of Selenate and Sulfate on Goethite. *Soil Sci. Soc. Am. J.* **66**, 1190–1197.

Zhang P. and Sparks D. L. (1990) Kinetics of selenate and selenite adsorption/desorption at the goethite/water interface. *Environ. Sci. Technol.* **24**, 1848–1856.
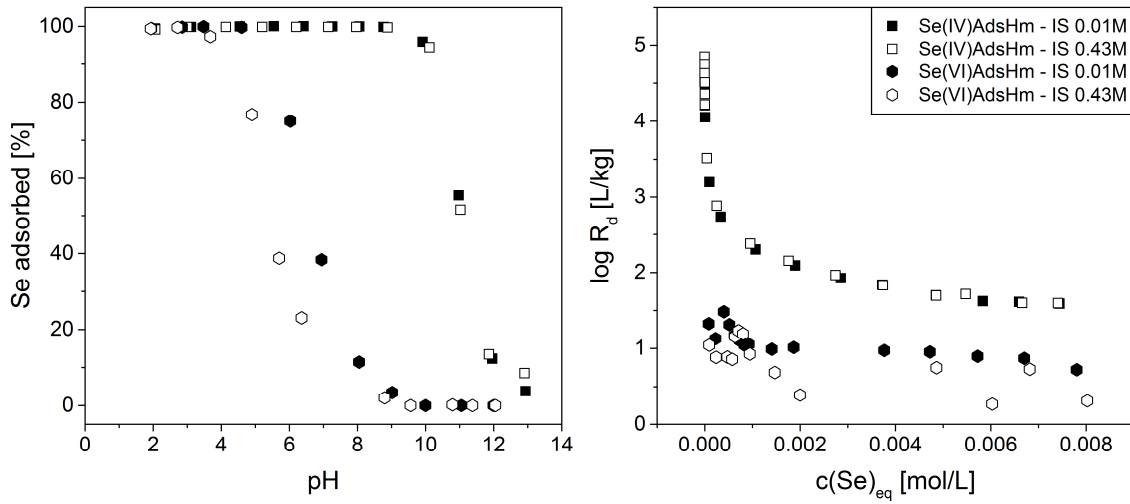
Fig. 1. Adsorption (Ads) of Se(VI) and Se(VI) by hematite (Hm) at m/V of 9.0 g/L. (Left) Se(IV) and Se(VI) adsorption onto hematite depending on pH and ionic strength (IS) at initial Se concentrations of 10^{-4} mol/L. (Right) Uptake of Se(IV) and Se(VI) by hematite at pH 7.5 as a function of the Se equilibrium concentration.
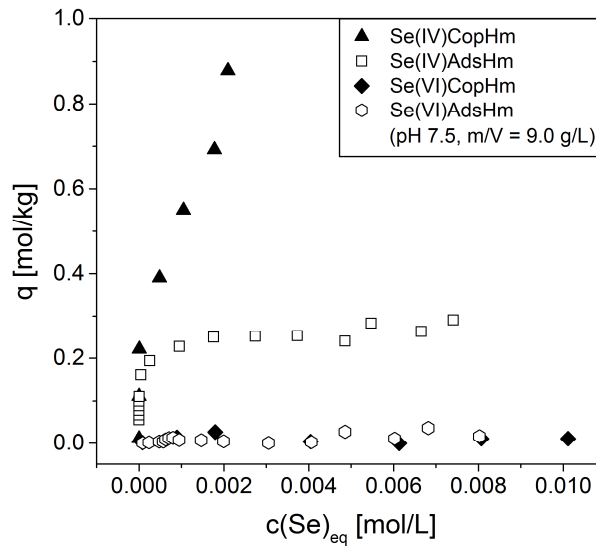
Fig. 2. Uptake of Se(IV) and Se(VI) by hematite (Hm) during coprecipitation (Cop) and adsorption (Ads) as a function of the Se equilibrium concentration.
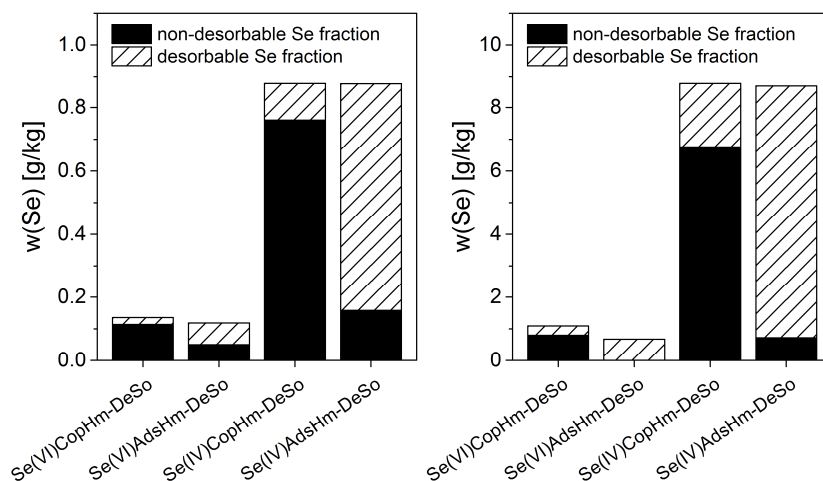
Fig. 3. Cumulative Se desorption from hematite adsorption (Ads) and coprecipitation (Cop) experiments after 3 washing steps at pH 12 (0.01 M KNO_3). Sorption conditions: m/V = 9.0 g/L; (Left) $c(Se)_{ini}$ = 10^{-4} mol/L ≈ ρ(Se) = 8 mg/L; (Right) $c(Se)_{ini}$ = 10^{-3} mol/L ≈ ρ(Se) = 80 mg/L.
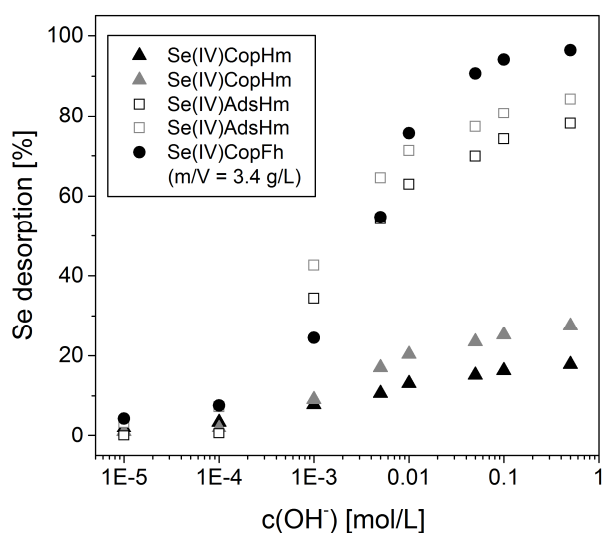
Fig. 4. Cumulative desorption of Se(IV) from hematite (Hm) and ferrihydrite (Fh) adsorption (Ads) and coprecipitation (Cop) experiments as a function of OH^- concentration. Initial Se concentration during the sorption step: $c(Se)_{ini}$ = 10^{-3} mol/L.
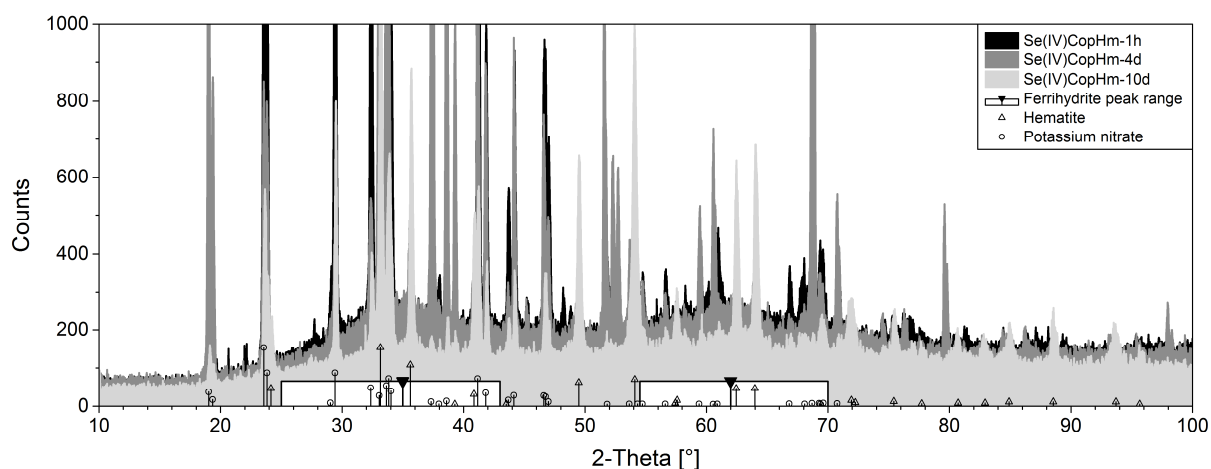
Fig. 5. Time-resolved XRD analysis (Cu Kα) of the transformation of 2-line ferrihydrite (broad peaks with maxima at 2θ of ~35° and ~62°) into crystalline hematite. Shown are 3 selected time steps for a series of Se(IV)

coprecipitated hematite samples ($c(Se)_{ini} = 10^{-3}$ mol/L). All peaks of crystalline phases are associated with hematite and KNO_3 (precipitated background electrolyte).
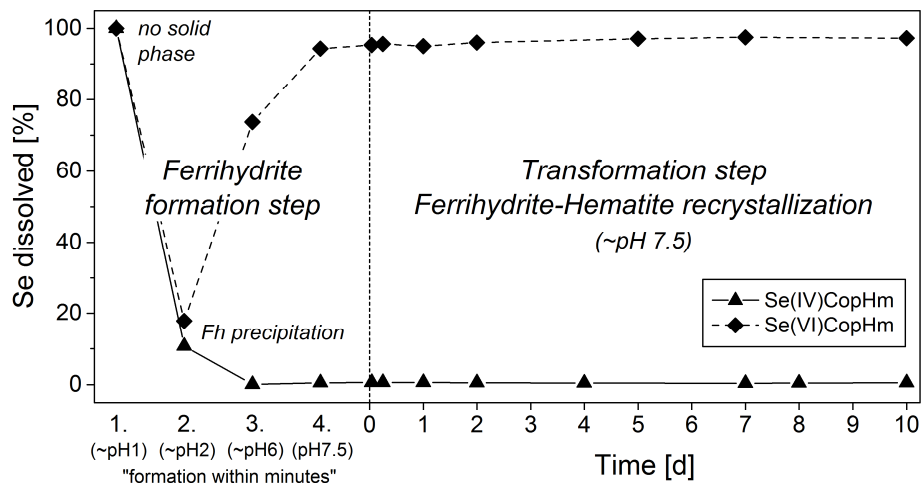

Fig. 6. Development of the Se concentration during the coprecipitation (Cop) of hematite (Hm). This includes the fast precipitation of the precursor phase ferrihydrite (Fh) in 4 steps and its subsequent transformation into hematite. Initial concentrations of Se(IV) and Se(VI): 10^{-3} mol/L.
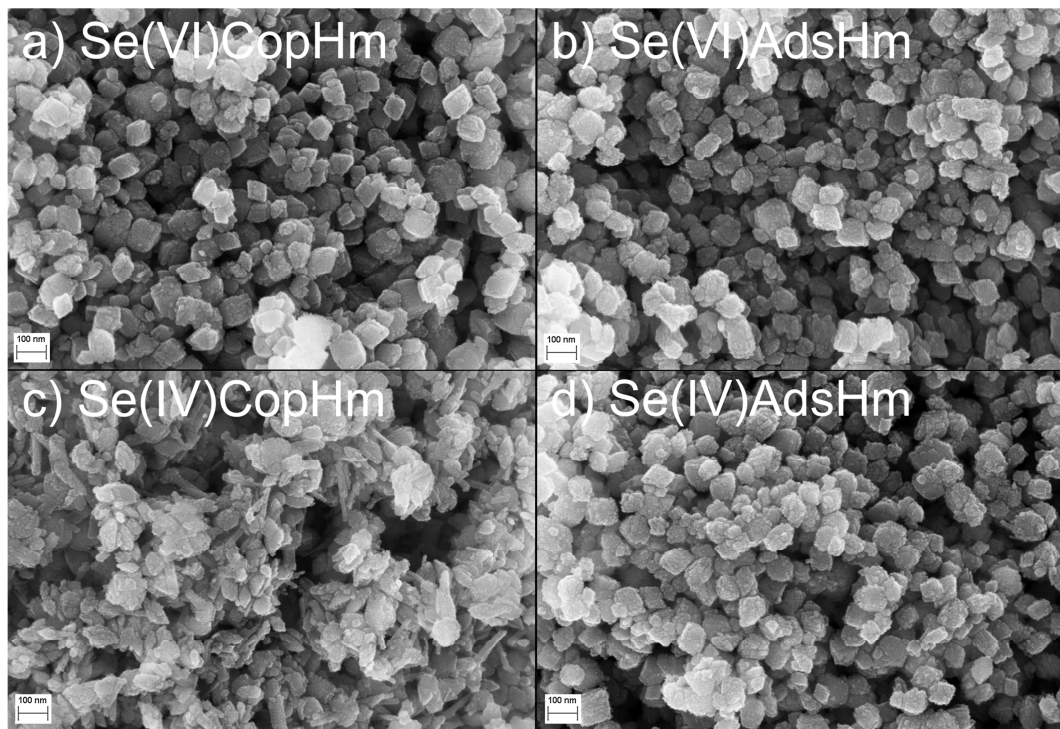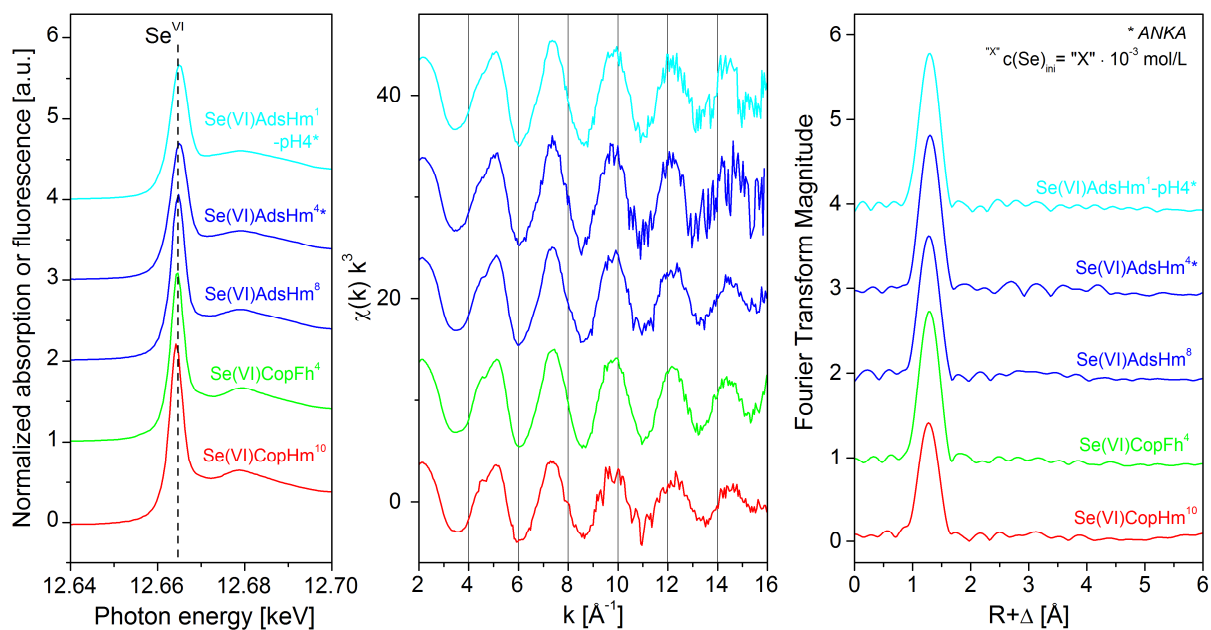

Fig. 7. SEM images of hematite (Hm) samples of coprecipitation (Cop) and adsorption (Ads) experiments with Se(VI) and Se(VI). Initial Se concentration of all samples: $4 \cdot 10^{-3}$ mol/L. (a) Se(VI) coprecipitation with hematite, (b) Se(VI) adsorption onto hematite, (c) Se(IV) coprecipitation with hematite; formation of a hematite-goethite mixed phase, (d) Se(IV) adsorption onto hematite
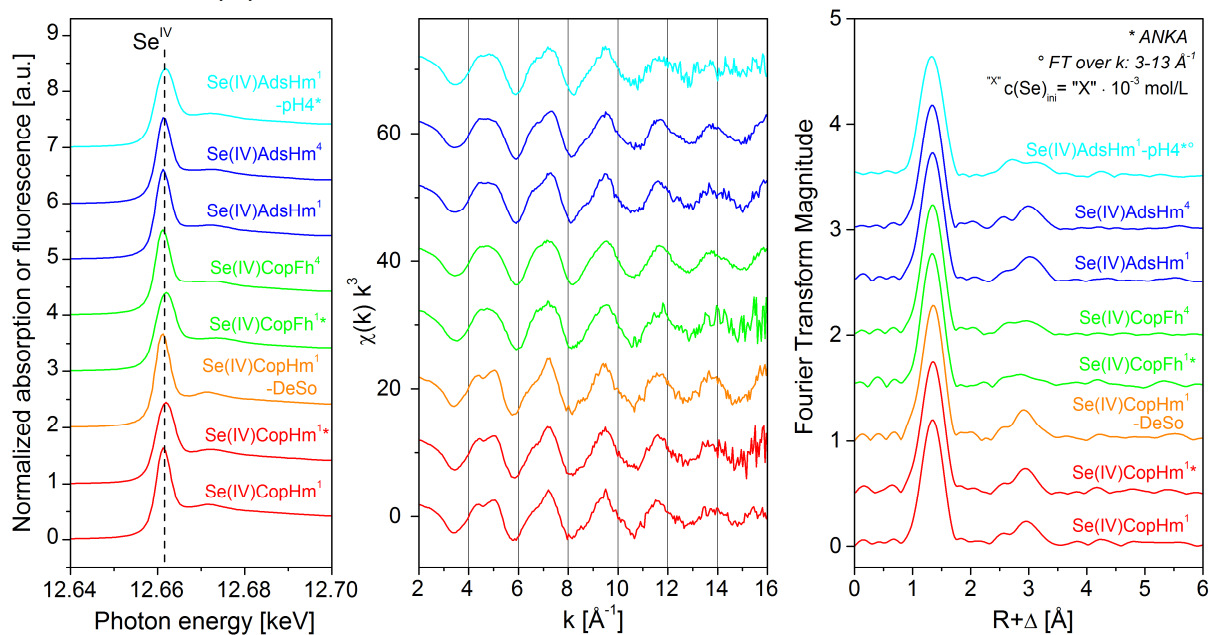
Interaction of Se(VI) with hematite

Se(VI)AdsHm[1]-pH4*
Se(VI)AdsHm[4]*
Se(VI)AdsHm[8]
Se(VI)CopFh[4]
Se(VI)CopHm[10]

* ANKA
"X" c(Se)$_{ini}$ = "X" · 10^{-3} mol/L

Interaction of Se(IV) with hematite

Se(IV)AdsHm[1]-pH4*
Se(IV)AdsHm[4]
Se(IV)AdsHm[1]
Se(IV)CopFh[4]
Se(IV)CopFh[1]*
Se(IV)CopHm[1]-DeSo
Se(IV)CopHm[1]*
Se(IV)CopHm[1]

* ANKA
° FT over k: 3-13 Å^{-1}
"X" c(Se)$_{ini}$ = "X" · 10^{-3} mol/L

Fig. 8. Se K-edge XANES and EXAFS spectra of Se(IV) and Se(VI) bearing hematite (Hm) and ferrihydrite (Fh) samples of different coprecipitation (Cop) and adsorption (Ads) studies. (If not otherwise indicated, EXAFS Fourier transforms (FT) were calculated over the k-range 3-14.5 Å^{-1})
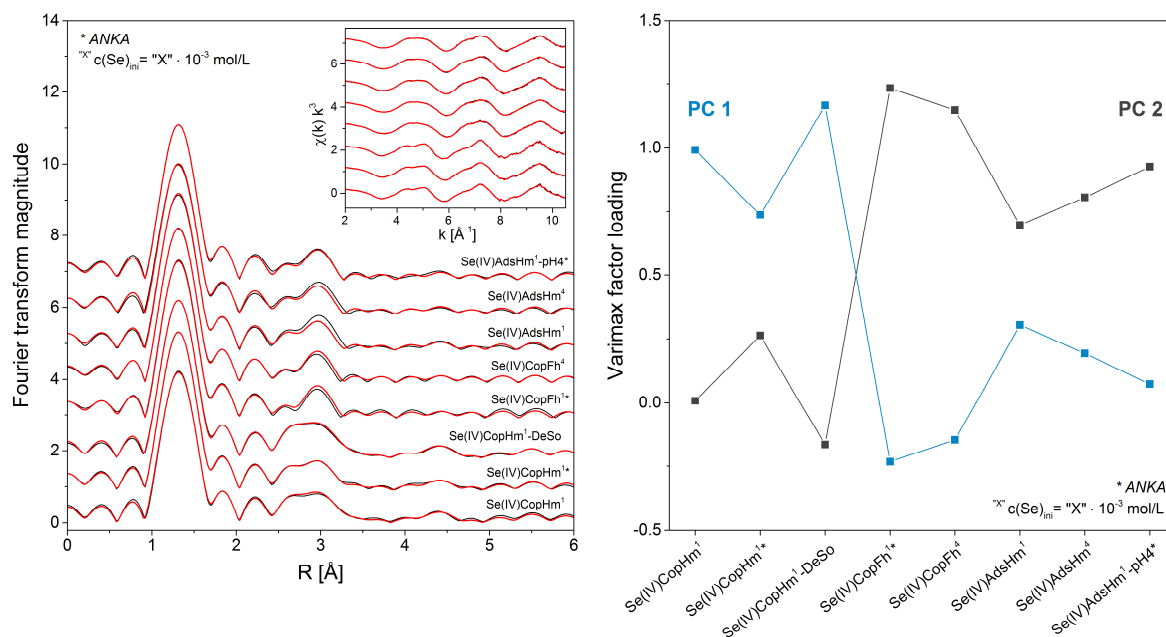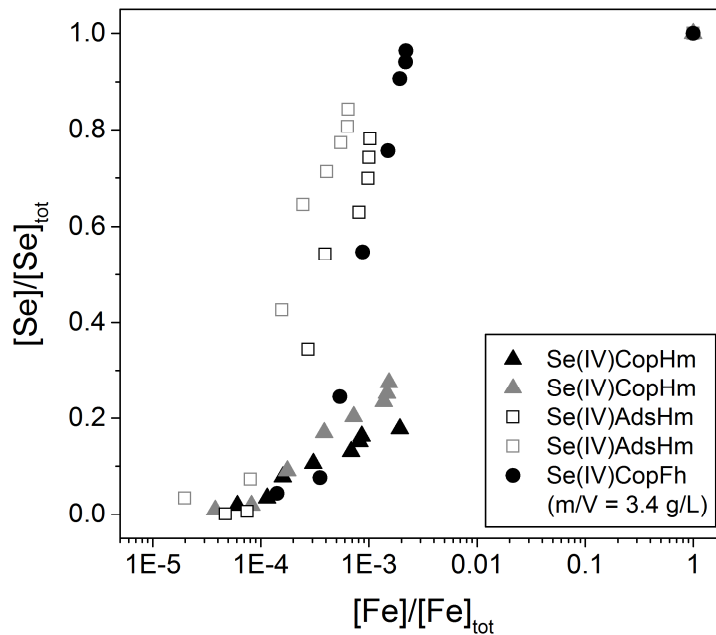
34

Fig. 9. Iterative transformation factor analysis of Se K-edge EXAFS spectra. Left: Experimental FT spectra (black lines) and their reconstruction (red lines) by two principal components (PC). EXAFS Fourier transforms were calculated over the k-range 2-10.5 Å^{-1}. Right: Varimax loadings of the spectral components.

Supplementary information

Dissolution of Fe vs. Se. Se(IV)-bearing hematite (Hm) and ferrihydrite (Fh) samples of previous adsorption (Ads) and coprecipitation (Cop) experiments were treated with varying [OH$^-$] solutions in the concentration range of 10^{-5} - 0.5 mol/L. In the last step, the iron oxides were completely dissolved by using a 6 M HCl.

Curti, E., Froideval-Zumbiehl, A., Guenther-Leopold, I., Martin, M., Bullemer, A., Linder, H., Borca, C.N. and Grolimund, D. (2014) Selenium redox speciation and coordination in high-burnup UO2 fuel: Consequences for the release of Se-79 in a deep underground repository. Journal of Nuclear Materials 453(1-3), 98-106.

Curti, E., Puranen, A., Grolimund, D., Jadernas, D., Sheptyakov, D. and Mesbah, A. (2015) Characterization of selenium in UO2 spent nuclear fuel by micro X-ray absorption spectroscopy and its thermodynamic stability. Environmental Science-Processes & Impacts 17(10), 1760-1768.

Scheinost, A.C. and Charlet, L. (2008) Selenite reduction by mackinawite, magnetite and siderite: XAS characterization of nanosized redox products. Environmental Science & Technology 42(6), 1984–1989.

Scheinost, A.C., Kirsch, R., Banerjee, D., Fernandez-Martinez, A., Zaenker, H., Funke, H. and Charlet, L. (2008) X-ray absorption and photoelectron spectroscopy investigation of selenite reduction by FeII-bearing minerals. Journal of Contaminant Hydrology 102(3-4), 228-245.